Journal of King Saud University – Science 34 (2022) 101739

Contents lists available at ScienceDirect

Journal of King Saud University – Science

journal homepage: www.sciencedirect.com

Original article

Chemical depolymerization of recycled PET to oxadiazole and hydrazone derivatives: Synthesis, characterization, molecular docking and DFT study

Nazia Tarannum [a,*], Rizwan Khan [a], Shoaiba Ansari [a], Ranu Agrawal [b], Swapnil Mishra [c], Mohd Ubaidullah [d], Abdulla A. Al-Kahtani [d]

[a] Department of Chemistry, Chaudhary Charan Singh University Meerut, Uttar Pradesh 250005, India
[b] Department of Applied Science, SCRIET, Chaudhary Charan Singh University Meerut, Uttar Pradesh 250005, India
[c] Centre for Bioinformatics, Allahabad University, Allahabad, Uttar Pradesh 211002, India
[d] Department of Chemistry, College of Science, King Saud University, Riyadh 11451, Saudi Arabia

ARTICLE INFO

Article history:
Received 11 August 2021
Revised 17 November 2021
Accepted 24 November 2021
Available online 29 November 2021

Keywords:
Polyethylene terephthalate
Terephthalic dihydrazide
Hydrazone
Oxadizole
DFT
Molecular docking

ABSTRACT

The extensive use of polyethylene terephthalate (PET)-based packaging materials has increased the desire to focus on their recycling. In this study, a chemical depolymerization method is proposed for synthesizing terephthalic dihydrazide (TDH) via the aminolysis of post-consumed PET. TDH is further used as a precursor along with 2-chlorobenzoic acid and 4-hydroxybenzoic acid to synthesize aromatic compounds, such as two oxadiazole derivatives, with potential applications. TDH is also used along with 2-chlorobenzaldehyde, benzaldehyde, and 4-hydroxybenzaldehyde to synthesize three hydrazone derivatives. The five compounds (the oxadiazoles and hydrazones) are well characterized by ultraviolet–visible (UV–Vis) spectroscopy, elemental analysis, Fourier-transform infrared (FTIR) spectroscopy, nuclear magnetic resonance (NMR), scanning electron microscopy (SEM), and thermal analysis. The theoretical parameters of the compounds are studied by *ab initio* density functional theory (DFT). The DFT calculations are conducted at Becke's three parameter and Lee–Yang–Parr (B3LYP) functional level of calculation with 631-G basis set. Moreover, several thermodynamic parameters at the ground state, such as the point group symmetry, dipole moment, and vibrational frequency, are calculated. The study of molecular docking of the synthesized compounds with target proteins (glucosamine-6-phosphate synthase (GlcN-6-P) and sterol 14α-demethylase (CYP51)) is conducted. Further, different parameters, such as the binding energy (BE), inhibition constant, internal energy, total intermolecular van der Waals forces, unbound energy, and hydrogen bond energy, are calculated. The three of the synthesized compounds are evaluated for antifungal and antibacterial activities using agar well diffusion method. The study of such compounds can offer a good prospective as potential antimicrobial and antifungal leads.

1. Introduction

The increasing concerns on sustainability have enhanced the interest in the use of recycled materials. PET is a widely available commercial polyester polymer, which is used nowadays as a packaging material (Sulyman et al., 2016). Only a very limited percentage of PET bottles are recycled, whereas the rest are disposed in landfills or incinerated (Webb et al., 2013). Therefore, facile and efficient methods of managing these post-consumed PET bottle wastes have been proposed (Sinha et al., 2010). The chemical and mechanical methods of recycling PET wastes have also been proposed (El Mejjatti et al., 2014). Moreover, the mechanical method (the collection, sorting, washing, and grinding of waste material) is the most common (Ragaert et al., 2017). Further, hydrolysis, glycolysis, methanolysis, ammonolysis, and aminolysis are well-established routes of recycling PET wastes chemically (Karpatiet al., 2019). Organocatalytic aminolysis, which produced a wide scale of crystalline terephthalamides, was demonstrated

* Corresponding author.
E-mail address: naz1012@gmail.com (N. Tarannum).
Peer review under responsibility of King Saud University.

Production and hosting by Elsevier

https://doi.org/10.1016/j.jksus.2021.101739
1018-3647/

in the attendance of 1,5,7- triazabicyclo(4,4,0)dec-5-ene (TBD) (Fukushima et al., 2013). Among the listed chemical degradation methods, aminolysis exhibits great potentials specifically in the presence of some chemicals, including ethylene diamine, hydrazine monohydrate, isophorone diamine, ethylene glycol, methylamine. The treatment of PET with these chemicals is preferred because they do not yield products that are susceptible to further modification (Shukla and Harad, 2006).

Here, a PET waste was chemically recycled with hydrazine monohydrate as the reagent. Thereafter, the obtained product was utilized to synthesize oxadiazole and hydrazone derivatives. These derivatives from the PET waste exhibited good antibacterial activity (Fahim et al., 2016; Agrawal et al., 2018). Agrawal et al. (2018) synthesized a new oxadiazole derivatives series from recycled PET by treating the waste with hydrazine monohydrate to yield TDH. Further, these oxadiazole derivatives exhibited good antimicrobial activity against *Bacillus cereus, Rhizopus, Candida albicans*, and *Escherichia coli* (Agrawal et al., 2018). Fahim et al. (2016) reported the synthesis of a chain of novel 1,3,4-oxadiazole, uracil, and derivatives of triazole, which exhibited antimicrobial and antioxidant activities, from PET (Fahim et al., 2016). Parab and Shukla (2013) reported the synthesis of 1,4-bis(5-aryl-1,3,4-oxadia zole-2-yl) benzene derivatives from TDH. In the synthesis, TDH was synthesized by the aminolysis depolymerization of waste PET with hydrazine monohydrate in the presence of catalysts ($MgCl_2$ and $NiCl_2$) under a reflux condition. Further, TDH was used as a precursor to synthesize 1,3,4 oxadiazole derivative (Parab and Shukla, 2013). Palekar et al. (2009) reported the synthesis of a novel series of 1,4-bis(6-(substituted phenyl)-[1,2,4]-triazolo[3,4-b]-1,3,4-thiadiazoles and 4-bis(substituted phenyl)-4-thiazolidinone derivatives from TDH, which was obtained from PET wastes. The synthesized compounds exhibited antibacterial activities against different fungal and bacterial strains.

Furthermore, oxadiazole and hydrazone are pharmacologically essential compounds. Oxadiazole comprises four different classes, although the most potent class is 1,3,4-oxadiazole, which comprises several biologically active molecules with various pharmacological relevance since 1,3,4-oxadiazole ring is susceptible to different nucleophilic and electrophilic substitution reactions (Patel et al., 2016). A profound literature review has revealed the benefit of structurally modifying 1,3,4-oxadiazole for synthetic and medicinal applications (Bharadwaj et al., 2017). Oxadiazole derivatives belong to the heterocyclic class of compounds, which have attracted tremendous interest in recent years. Their chemistry and applications have been reported (Bansal et al., 2014; Kazi, 2014). Hydrazones containing an azomethine (–NHN=CH) proton constitutes an essential group of compound for the evolution of new drugs (Rollas and Küçükgüzel, 2007) owing to their pivotal role in rendering a compound biologically active. Hydrazones, which are synthesized by refluxing acid hydrazides with relevant carbonyl compounds, exhibit different application potentials owing to their biological activities, as well as their metal complexing and corrosion inhibiting capacities (Patel et al., 2016; Bansal et al., 2014). Hydrazones have inspired researchers to synthesize their novel derivatives owing to their providential bioactivity and efficacy in medicinal chemistry (Bharadwaj et al., 2017). The general structures of oxadiazole and hydrazone are shown in Fig. S1.

In this work, the depolymerization of post-consumed PET bottles by aminolysis to produce TDH, which was further converted into potentially applicable and economical aromatic amide was attempted. The two oxadiazole derivatives were synthesized by reacting TDH with 2-chlorobenzoic acid/4-hydroxybenzoic acid. The three hydrazone derivatives, which were reported here, have been prepared from TDH along with 2-chlorobenzaldehyde/benzaldehyde/4-hydroxylbenzaldehyde as the reactants. The oxadiazole and hydrazone derivatives were characterized by UV–Vis spectroscopy, FTIR, NMR, elemental analysis, SEM, and thermal analysis. Amongst five, three of the synthesized compounds were evaluated for antifungal as well as antibacterial activity *in vivo*.

The molecular docking study of the synthesized compounds was performed by *in silico* analysis for targeting proteins, i.e., GlcN-6-P and CYP51. GlcN-6-P is specifically known as L-gluta mine:D-fructose-6-phosphate (Fru-6-P) amidotransferase (EC 2.6.1.16) (Chmara et al., 1984). This enzyme metabolizes hexosamineby converting Fru-6-P into GlcN-6-P.In this reaction, which ultimately yields N-acetylglucosamine (NAG), glutamine acts as the ammonia source. NAG (peptidoglycan in bacteria and chitin and mannoproteins in fungi) is an essential component of their cell walls (Milewski et al., 1988). CYP51 is belongs to the cytochrome P450 superfamily and is essential for fungal viability (Vanden and Koymans, 1998). This enzyme is an essential target for designing antifungal agents since it functions as a biocatalyst in the biosynthesis of ergosterol in fungi which is the main constituent of the fungal cell wall. During the biosynthesis, the methyl group is removed from the C-14 position of the sterol molecule (Yoshida et al., 2000). Furthermore, the synthesized oxadiazole and hydrazone derivatives exhibit many medicinal properties, such as antifungal (Mishra, 2014), antitumor (Bondock et al., 2012), antimicrobial (Rollas et al., 2002), antitubercular (-Kaymakçıoğlu and Rollas, 2002), anticancer, and anti-inflammatory (Farghaly et al., 2000) properties, as well as many pharmacological activities (Popiołek, 2017). Oxadiazoles also exhibit herbicidal, pesticidal, analgesic, and plant growth regulatory activities (Patel et al., 2016). Further, DFT was performed for the theoretical study. DFT is a popular theoretical modeling tool since the 1970s. It predicts a wide range of molecular properties, such as molecular structures, vibrational frequencies, ionization energies, atomization energies, magnetic and electric properties, and reaction pathways (Saeed et al., 2013). Here, all the DFT computation were performed at Becke's three-parameter and the Lee–Yang–Parr (B3LYP) functional levels with a 631G basis set to optimize the geometries of the ground states of the five synthesized compounds (the oxadiazole and hydrazone derivatives). The vibrational frequencies of the compounds were also calculated.

2. Materials and method

2.1. Chemicals

The post-consumed plastic and soft-drink bottles were obtained and utilized after pretreatment. Hydrazine monohydrate (90%) was purchased from Fisher Scientific (USA), and2-chlorobenzaldehyde and 4-hydroxybenzaldehyde were purchased from CDH Fine Chemical (India). Methanol, dimethylsulfoxide, and benzaldehyde were procured from Fisher Scientific; 2-chlorobenzoic acid was procured from SD Fine Chemical (India); and 4-hydroxybenzoic acid was procured from Sisco Research Laboratories (India). Ciprofloxacine was procured from Fisher Scientific

2.2. Instrument

Elemental analysis was done using Thermo Scientific (FLASH 2000) CHN Elemental Analyser). UV–Vis spectroscopy was done on a Systronics double beam spectrophotometer 2201. The FTIR spectra of the compounds were analyzed on a Cary 630 FTIR spectrometer (Agilent Technologies). NMR (H^1 and C^{13} NMR) were performed on a Bruker Avance III (400 MHz) NMR spectrometer. Deuterated DMSO was used as the NMR solvent. SEM was performed on a ZEISS scanning electron microscope. Differential scanning calorimetry (DSC) was conducted on DSC7020 thermal analysis system (Hitachi). Further, thermogravimetry/differential

thermal analysis (TG/DTA) was performed on Perkin Elmer Diamond TG/DTA at 20 °C/min in a nitrogen atmosphere.

2.3. Method

2.3.1. Pretreatment of PET

The obtained post-consumed PET bottles were cut into small flakes, which were washed successively in boiling water and methanol before they were dried in an oven at ~70 °C (Agrawal et al., 2016).

2.3.2. Synthesis of TDH

TDH was synthesized, as discussed elsewhere (Agrawal et al., 2018). Briefly, the starting material was obtained, as discussed in Section 2.3.1. The processed PET flakes were dried for 5 h at 80 °C. Thereafter, the flakes were incubated with hydrazine monohydrate in a 1:10 (w/v) ratio. The reaction flask was sealed, and the reaction was performed with continuous stirring for 24 h at ambient temperature and pressure. PET was aminolyzed during the reaction, and the obtained product (TDH) was separated and washed with distilled water. Afterward, the obtained precipitate was dried in an oven.

2.3.3. Synthesis of the oxadiazole derivatives

2.3.3.1. Synthesis of 1,4-bis[5-(2-chlorophenyl)-1,3,4 oxadiazole-2-yl] benzene (OCB). A solution of TDH (19.2 g in 100 mL of DMSO) was added to 2-chlorobenzoic acid (31.5 g), and the reaction mixture was refluxed for 25 min at 175 °C. The color of the reaction mixture was brown. After the reaction, the mixture was filtered, and the precipitate was vacuum dried at 60 °C and washed successively with methanol and hot water. The precipitate was vacuum-dried again for 6 h at 70 °C. The percentage yield of OCB was 56.41%.

2.3.3.2. Synthesis of 1,4 bis [5(4-hydroxy phenyl)–1,3,4 oxadiazole-2-yl]benzene (OHB). A TDH solution (19.2 g in 100 mL of DMSO) was added to 27.6 g of 4-hydroxybenzoic acid, and the reaction mixture was refluxed for 35 min at 175 °C. The color of the reaction mixture was pale yellow. Afterward, the reaction mixture was filtered, and the precipitate was vacuum-dried at 60 °C and washed successively with methanol and hot water. The precipitate was vacuum-dried again for 6 h at 70 °C. The percentage yield of OHB was 49.31%.

2.3.4. Synthesis of the hydrazone derivatives

2.3.4.1. Synthesis of N,N′-bis(2-chlorobenzaldehyde)terephthalohydrazide (TCA). A solution of TDH (19.2 g in 100 mL of DMSO) was added to 30 mL of 2-chlorobenzaldehyde, and the reaction mixture was refluxed at 165 °C, after which it precipitated immediately. The color of the reaction product was pale yellow. The reaction mixture was filtered, and the precipitate was vacuum-dried at 60 °C, after which it was washed successively with methanol and hot water. The precipitate was vacuum-dried again for 6 h at 65 °C. The percentage yield of TCA was 73.36%.

2.3.4.2. Synthesis of N,N′-bis(benzylidene)terephthalohydrazide (TBA). A TDH solution (19.2 g in 100 mL of DMSO) was added to 22 mL of benzaldehyde, and the reaction mixture was refluxed for 15 min at 165 °C. The reaction mixture, which was pale yellow, was filtered, and the precipitate was vacuum-dried at 60 °C, after which it was washed successively with methanol and hot water. The precipitate was vacuum-dried again for 6 h at 65 °C. The percentage yield of TBA was 73.89%.

2.3.4.3. Synthesis of N,N′-bis(4-hydroxybenzylidene)terephthalohydrazide (THD). A TDH solution (19.2 g in 100 mL of DMSO) was added to 24.2 g of 4-hydroxy benzaldehyde, and the reaction mixture was refluxed for 15 min at 165 °C. The reaction mixture, which was pale yellow, was filtered, and the precipitate was vacuum-dried at 60 °C and washed successively with methanol and hot water. The precipitate was vacuum-dried again for 6 h at 165 °C. The percentage yield of THD was 54.97 %.

2.3.4.4. In silico molecular docking. The study of molecular docking was conducted with the default setting of standard precision (SP). The selection of the best pose was according to the minimum BE and interactions with the respective protein. The AutoDock 4.2 software was employed for the molecular docking. The Lamarckian genetic algorithm with a population size of 150 and a crossover rate of 0.8 was employed for the molecular docking. Molecular docking was exhaustively performed by increasing the number of runs to 100 to increase the repetitiveness of the poses for increased accuracy. The selection of the best outcome was based on the pose of the ligand inside the cavity, the minimum BE, and the interactions with the respective protein. Chimera was employed to visualize the interaction between the protein–ligand complexes (Bharadwaj et al., 2017).

Ligand preparation: The chemical structures of OCB, OHB, TCA, TBA, and THD, as well as those of the ligands, were drawn with the ChemSketch tool, after which they were optimized with the PRODRG server. The PDB file of voriconazole was retrieved from the DrugBank (www.drugbank.ca).

Protein preparation: The three-dimensional (3D) structures of the proteins (1. GlcN-6-P from *Escherichia coli* (PDB ID: 1JXA) and 2. CYP51B from a pathogenic filamentous fungus *Aspergillus fumigatus* (PDB ID: 4UYL) were downloaded from the Protein Data Bank (https://www.rcsb.org/). Afterward, the water molecule and heteroatoms were deleted from the PDB files.

2.3.4.5. DFT study. The computer simulations were performed with a GAUSSIAN 03 program package (Frisch et al., 2004). The DFT (Kohn and Sham, 1965; Becke, 1993) computation were performed at B3LYP level of calculation. Furthermore, a 631-G basis set was utilized for the optimization of the ground-state geometry.

2.3.4.6. Culture maintenance. The fungal species *Aspergillus niger, Aspergillus fumigatus, Pennicillium* sp., *Candida albicans* and *Mucor* were cultured in the laboratory on SDA (Sabouraud Dextrose Agar) media in presence of streptomycin antibiotic. The bacterial species *Escherichia coli and Bacillus cereus* were cultured on the nutrient agar medium in the laboratory.

2.3.5. Antifungal activity

OHB, TBA and THD were evaluated for antifungal activity by using agar well diffusion method (Akhtar et al., 2008) against the following fungal species viz., *Aspergillus niger, Aspergillus fumigatus, Pennicillium* sp., *Candida albicans* and *Mucor.* OCB and TCA could not be evaluated due to not dissolving in DMSO. Zone of inhibition of fungal growth were measured using 1 mg/mL concentration of OHB, TBA and THD made in DMSO. The method was followed as described in the earlier paper (Agrawal et al., 2017). The antifungal activity of compounds were compared with fluconazole (Bakht et al., 2010) and DMSO blank using as positive control as negative control, respectively. Each experiment was set as triplicate and results were recorded as an average and standard deviation.

2.3.6. Antibacterial activity

OHB, TBA and THD were also analysed for antibacterial activity using agar well diffusion method (Tomi et al., 2013) as discussed above against two bacterial strains viz., *Escherichia coli* and *Bacillus cereus*. *Bacillus cereus* is a Gram positive bacteria, while *Escherichia coli* is a Gram negative bacteria.1 mg/mL concentrations of OHB, TBA and THD were made in DMSO and antibiotic ciprofloxacin

was used as reference antibacterial agent (Sheehan et al., 1999). OCB and TCA could not be evaluated due to insolubility in DMSO. By calculating the zone of inhibition, antibacterial activity was also determined. Each experiment was set as triplicate and the average and standard deviation of the results were reported.

3. Results and discussion

3.1. Chemistry of the synthesis

The PET flakes were degraded with hydrazine monohydrate by a simple aminolysis reaction without any catalyst under pressure and ambient temperature conditions. The reaction proceeded via a nucleophilic mechanism. The amines of hydrazine acted as a nucleophile, which reacted with the carbonyl group of PET to break the ester linkage and produce ethylene glycol as the by-product. The structure of TDH is proposed in Fig. 1, while those of the oxadiazole and hydrazone derivatives are proposed in Fig. 2. TDH and a substituted benzoic acid act as the precursors for synthesizing oxadiazole, thus forming a product with a heterocyclic ring. The substituted benzaldehyde reacts with amine group of TDH thereby causing nucleophilic addition to form hydrazone. Based on the elemental analysis, UV–Vis spectroscopy, FTIR spectroscopy, NMR spectroscopy, SEM, and thermal analysis, the chemical structures of the synthesized compounds correlated with the expected theoretical structure.

3.2. Characterization

3.2.1. General properties

The synthesized compounds were obtained in powder forms. The melting temperatures of the compounds were >300 °C. The solubility of the synthesized compounds was tested in different solvents, as listed in Table S1. The solubility data indicated that the chloro-substituted oxadiazole was partially soluble in chloroform and trifluoroacetic acid (TFA) when heated, whereas the hydroxyl-substituted oxadiazole exhibited partial solubility in DMSO and TFA and carbon tetrachloride when heated. Upon heating, the hydrazone derivatives (TBA and THD) became soluble in DMSO exhibited partial solubility in chloroform.

3.3. Elemental analysis

CHNS analysis helped to identify the percentages of carbon, hydrogen, nitrogen, and sulfur in the oxadiazole and hydrazone derivatives. Table S2 presents the comparison of the results obtained from the experimental and theoretical elemental analyses of the synthesized compounds. The percentages of the experimental and theoretical elemental data correlated and established the structures of the synthesized oxadiazole and hydrazone compounds well.

3.4. UV–Vis spectroscopy

The UV–Vis spectra of the compounds (OHB, THD, and TBA) were analyzed by irradiating their solutions in DMSO of the same concentrations (0.1 mg/mL) in a 1-cm-path quartz cell. The oxadiazole derivatives exhibited strong absorptions at 356 nm, while the hydrazone compounds exhibited strong absorptions in the range of 346–351 nm.

3.5. FTIR analysis

The FTIR spectrum of TDH has been discussed elsewhere (Agrawal et al., 2018). It exhibited absorption bands at 3310 and 1602 cm^{-1}, which were attributed to N–H and C=O stretchings, respectively. Further, the FTIR spectra of an oxadiazole derivative (OCB) exhibited absorption bands at 3198 and 3015 cm^{-1}, which were assigned to the C–H (Ar) symmetric and asymmetric stretches, respectively. The absorption bands at 1653 and 1591 cm^{-1} were attributed to C=N and C=C stretchings, which indicated the presence of the imine and aromatic rings, respectively. The bands at 1265 and 741 cm^{-1} corresponded to the =C–O and C–Cl stretchings, respectively. OHB exhibited absorption bands, which were attributed to O–H and C–H stretchings at 3198 and 3015 cm^{-1}, respectively. The absorption bands at 1647 and 1592 cm^{-1} were attributed to the C=N and C=C stretchings, which indicated the presence of the imine and aromatic rings, respectively. The band at 1235 cm^{-1} exhibited the =C–O stretching. Fig. S2 shows the FTIR spectra of the oxadiazole derivatives.

The FTIR spectra of the hydrazone derivatives (TCA, TBA, and THD) were recorded, as shown in Fig. S3. TCA exhibited absorption bands, which were attributed to the N–H, C=N (imine), and C=O stretching at 3203, 1645, and 1592 cm^{-1}, respectively. The absorp-

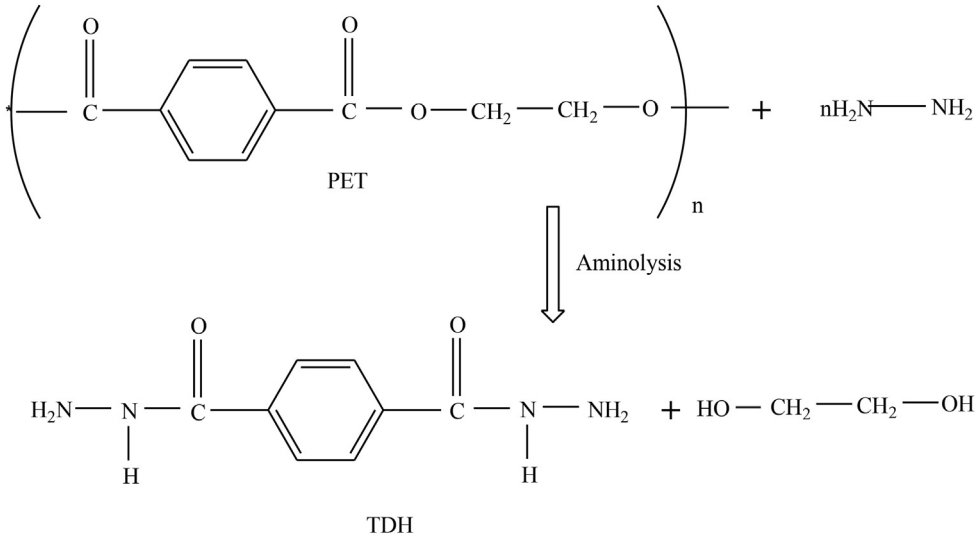

Fig. 1. Synthesis of TDH via the aminolysis of PET waste.

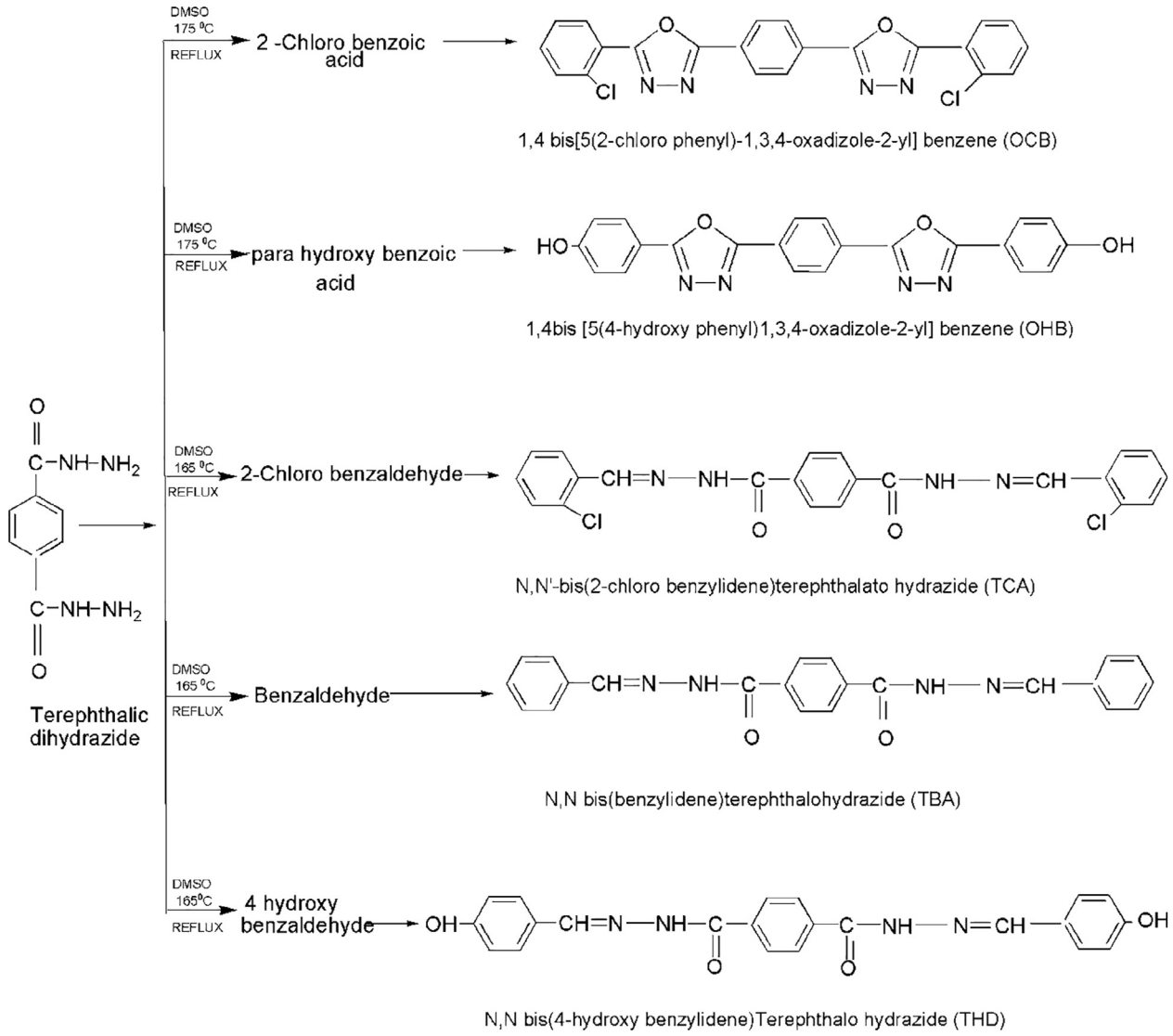

Fig. 2. Synthesis of the two oxadiazole derivatives (OCB and OHB) and three hydrazone derivatives (TCA, TBA, and THD).

tion bands at 1542 and 3058 cm^{-1} corresponded to the C=C and C–H stretching, which indicated the presence of an aromatic ring. The bands at 749 and 721 cm^{-1} corresponded to C–Cl stretching. TBA displayed absorption bands at 3232, 1647, and 1604 cm^{-1}, which were attributed to N–H, C=N (imine), and C=O stretching, respectively. The bands at 1552 and 3035 cm^{-1} revealed the C=C and C–H stretching, indicating the presence of an aromatic ring, respectively. The band at 1278 cm^{-1} exhibited a C–N stretching. Furthermore, THD exhibited absorption bands at 3423, 1609, and 1602 cm^{-1}, which were attributed to N–H, C=N (imine), and C=O stretching, respectively. The band at 3042 cm^{-1} revealed a C–H stretching, which indicated the presence of an aromatic ring. The absorption band at 1268 cm^{-1}also revealed a C–N stretching. The band at 3200 cm^{-1} exhibited the O–H stretching. Fig. S3 shows the FTIR spectra of the hydrazone derivatives.

3.6. NMR characterization

The ^{1}H and ^{13}C NMR spectra of OHB, TBA, and THD are shown in Figs. S4 and S5, respectively. ^{1}H NMR, and the ^{1}H and ^{13}C NMR spectra OCB and TCA were not observed due to the solubility setbacks (Table S1). Deuterated DMSO was utilized as the solvent for NMR analysis. The peaks, which were observed in ^{1}H NMR spectrum of OHB, revealed a sharp singlet at δ 7.3, which is typical for Ar–H protons. The peaks, which were observed in ^{1}H NMR spectra of TBA and THD, were identified at δ 3.5 as sharp singlets owing to N–NH protons, and the peak at δ 7.3 is typical for four Ar–H protons. A sharp singlet at δ 2.5 was owing to the solvent.

^{13}C NMR spectrum of OHB showed a sharp singlet at δ 78 for C–O–C (heterocyclic compounds). The peaks in ^{13}C NMR spectra of TBA and THD were designated as a sharp singlet at δ146 owing to the C=O group, whereas the peak at δ(125–135) are typical for the four aromatic groups. Fig. S4 and Fig. S5 show ^{1}H and ^{13}C NMR spectra of OHB, TBA, and THD. A sharp singlet at δ40 was owing to DMSO.

3.7. SEM

SEM is an extensively used technique for studying the morphological structure and surface characteristics of a compound. Fig. S6 shows SEM images of OCB and OHB, whereas Fig. S7 shows those of THD, TBA, and TCA. As revealed by SEM, the surface characteristics of the oxadiazole derivatives revealed their amorphous nature.

3.8. Thermal analysis

TGA of the oxadiazole and hydrazone derivatives were measured at 20 °C/min employing the following average weights of the sample: OCB, 5.380 mg; OHB, 4.370 mg; TCA, 6.496 mg; TBA, 6.047 mg; and THD, 6.687 mg. TGA was conducted to offer an insight into the structures and properties of the oxadiazole and hydrazone derivatives with respect to the temperature (Agrawal et al., 2018). Their weight losses were observed after 150 °C (Figs. S8 and S9). OCB exhibited a 35% weight loss upto 200 °C, whereas OHB exhibited a 14% loss. Fig. S8 shows the well-defined processes of their weight losses. Moreover, THD exhibited several weight loss processes. The three hydrazone derivatives exhibited weight losses of upto 15% until 200 °C. Among the hydrazone derivatives, TCA and TBA exhibited minimum weight losses of 5%–6% upto 350 °C, whereas THD exhibited a 32% weight loss for upto 350 °C.

Further, DSC was performed with 6 mg of each sample at an ambient temperature for upto 700 °C at a heating rate of 20 °C/min in a nitrogen atmosphere. The melting temperature of TBA was observed between 355 °C and 380 °C, and the observed melting enthalpy were 165.97 and 115.77 J/g, respectively. However, the melting temperatures and enthalpies of TCA were 363 °C and 688.45 J/g, respectively, as shown in Fig. S10. The presence of endothermic peaks in TBA and TCA confirmed the semicrystalline structures of the hydrazone derivatives (Figs. S7 (a) and (b) (Gaabour, 2017). DSC analyses of the other three samples were not conducted because their melting temperatures exceeded 350 °C. DSC results of TCA and TBA (Fig. S10) revealed endothermic peaks, which were overlapped with the TGA results, thereby indicating that this process was more related to the heat that was adsorbed from degrading the samples rather than from melting them. Since the atmosphere was inert, the degradation process relied mainly on bond breaking, which is typically an endothermic process. Additionally, the peaks of DSC curve of TBA indicated two-step degradation, and the derivative curve of the TG curve confirmed it.

3.9. DFT study

The DFT calculations were conducted at the B3LYP level with a 631-G basis set to optimize the ground-state geometries of the five compounds (TCA, TBA, THD, OCB, and OHB). Some calculated thermodynamic parameters in the ground states (point group symmetry, dipole moment, and zero-point vibrational energy (ZPVE)) of the compounds are presented in Table S3. The presence of an –OH group in OHB and THD pulled the electrostatic fields, which increased their dipole moments. The molecules possessed a C1 symmetry with the lowest energy at all levels. The total energy of the molecules was the sum of translational, rotational, vibrational, and electronic energies. The vibrational frequencies of the five compounds were optimized by DFT and correlated with the experimental FTIR data. Their theoretical and experimental vibrational frequencies corresponded, thus establishing the structure. The supplementary data (Table S4) of the calculated vibrational frequencies of the compounds are presented (Saeed et al., 2013; Teotia et al., 2019).

3.10. Molecular docking

The molecular docking studies of OCB, OHB, TCA, TBA, and THD were performed with target proteins (GlcN-6-P (1jxa) and CYP51 (4uyl) (Fig. 3(a) & (b). GlcN-6-P enzyme is pivotal to the formation of the cell walls of bacteria and fungi. GlcN-6-P has been proven as a potent target for synthesizing antifungal agents (Wojciechowski et al., 2005; Sarojini et al., 2010; Bharadwaj et al., 2017). CYP51 is a potential target site for establishing an antifungal agent, such as voriconazole. Therefore, voriconazole was employed as a reference with the five ligands for the docking study against CYP51 to compare their BEs and poses. GlcN-6-P binding site is formed by the loop with a highly flexible area and without a very deep pocket. Owing to its shallow nature, the cavity is generally exposed to the water and lipophilic residues in the region, as well as to some hydrophobic residues in the interior. The five ligands possessed minimum BEs of −4.48 to −8.30 kcal/Mol, the same poses inside their cavities, and noncovalent interactions along with the formation of hydrogen bonds with the cavity residues (Table S5 and Fig. 4(i)–(v)).

BE of the interaction between voriconazole and GlcN-6-P was −7.03 kcal/Mol, and no hydrogen bonds were formed with cavity residues. It was observed that BEs of voriconazole was very close to those of the five ligands with GlcN-6-P. The key residues that interacted inside the cavities were Thr302, Gln348, Ser347, Ser401, Glu488, Ala602, Lys603, Ser604, and Val605. The ligands (OCB, OHB, TCA, TBA and THD), along with the reference (voriconazole), were docked within the cavity of 4uyl. The heme-containing binding site in the protein possessed sufficient space and volume, which could easily accommodate the ligands. The interactions between the cavity residues, heme, and ligands were owing to the interactions of non covalent in addition to the hydrogen bonds, to achieve proper bonding. The five compounds possessed good BEs from −8.12 to −11.96 kcal/Mol and were comparable with those of voriconazole with the target protein (4uyl). Further, it was observed that Ala307, His310, Leu508, His374, Ser375,

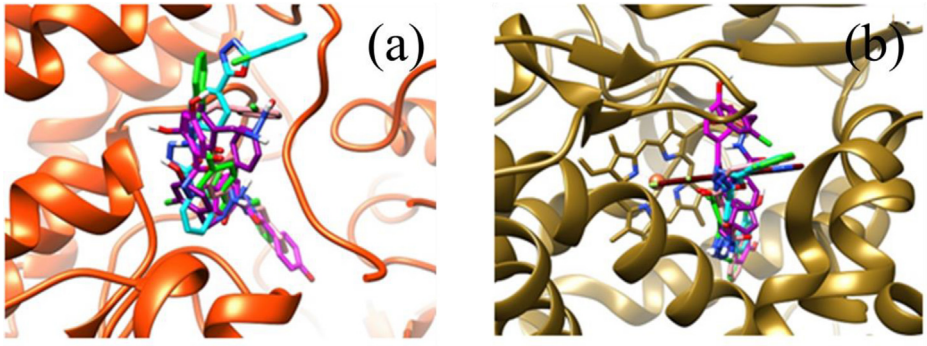

Fig. 3. (a) The ligands focused in the cavities of the target proteins (the orange ribbon represents the target (GlcN-6-P) protein (1jxa), and the five ligands are shown in stick forms with different colors inside the protein cavity, while (b) the green ribbon indicates the target protein CYP51 (4uyl) with six ligands inside the cavities. The heme group is represented by the orange ball).

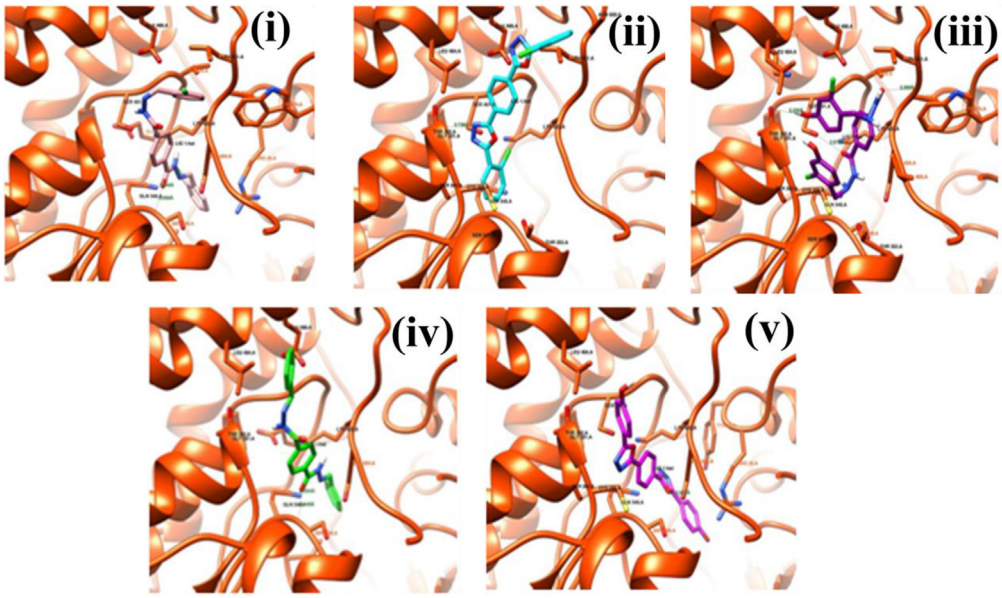

Fig. 4. Poses of the ligands inside the target protein CYP51 (1jxa). The interacting residues were labeled and the intermolecular hydrogen bonds were represented by lines labeled with their distance. (i), (ii), (iii), (iv), and (v) show OCB (cyan), OHB (purple), TCA (pink), TBA (green), and THD (blue) inside the cavity of 1jxa (orange ribbon), respectively.

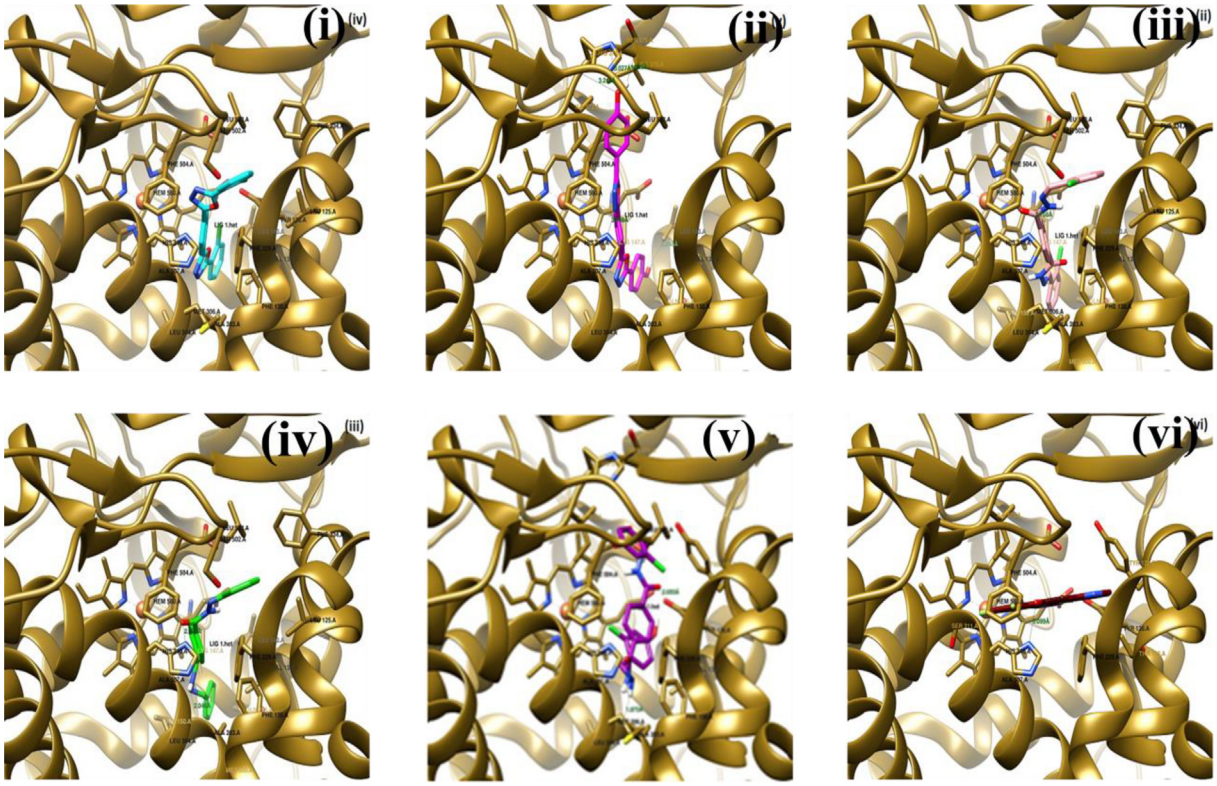

Fig. 5. Poses of the ligands inside the target protein CYP51 (4uyl). The interacting residues were labeled, and the intermolecular hydrogen bonds were represented by lines labeled with the distance. (i), (ii), (iii), (iv), (v), and (vi) show OCB (cyan), OHB (purple), TCA (pink), TBA (green), THD (blue), and Voriconazole (red) inside the cavity of 4uyl (green ribbon), respectively.

Ile373, Phe504, and Leu503 residues demonstrated close interactions with the ligands while binding (Table S6 and Fig. 5(i)–(v)). Therefore, the molecular docking studies implied that both classes of the synthesized compounds (the oxadiazole and hydrazone derivatives) might exhibit good antifungal activity.

3.11. Antifungal activity

Antifungal activity of OHB, TBA and THD (1 mg/mL) was evaluated against fungal species *Aspergillus niger, Aspergillus fumigatus, Pennicillium, Candida albicans* and *Mucor*. The activity was

Table 1
Determination of zone of inhibition in presence of 1 mg/mL concentration of oxadiazole and hydrazone derivatives against different fungal species (fluconazole as reference and DMSO as blank).

Compound	Concentration	Zone of inhibition (mm)				
		Aspergillus niger	*Aspergillus fumigatus*	*Pennicillium* sp.	*Candida albicans*	*Mucor*
OHB	(1 mg /mL)	29 ± 1.414	16 ± 0	23 ± 1.414	18.5 ± 2.121	21.75 ± 1.06
TBA	(1 mg/mL)	15.75 ± 0.353	13.5 ± 0.707	18 ± 1.414	18 ± 2.828	24 ± 0
THD	(1 mg/mL)	26.5 ± 2.121	10.75 ± 0.353	19.5 ± 2.121	21 ± 0	22 ± 1.414
Fluconazole	(1 mg/mL)	5.0 ± 1.414	7.5 ± 0.707	5.5 ± 0.707	12.25 ± 0.353	10.5 ± 0.707
DMSO	Solvent	0	0	0	0	0

Table 2
Determination of zone of inhibition in presence of 1 mg/mL concentration of oxadiazole and hydrazone derivatives against different bacterial species (ciprofloxacin as reference and DMSO as blank).

Compound	Concentration	Zone of inhibition (mm)	
		Escherichia coli	*Bacillus cereus*
OHB	(1 mg/mL)	14.5 ± 0.707	8.5 ± 0.707
TBA	(1 mg/mL)	13.25 ± 0.353	7.5 ± 2.121
THD	(1 mg/mL)	15 ± 1.414	8.5 ± 2.121
Ciprofloxacin	(1 mg/mL)	34 ± 2.828	24 ± 2.828
DMSO	Solvent	0	0

expressed in term of zone of inhibition in given Table 1. Obtained results explained that all synthesized compounds have shown good antifungal activity in comparison to fluconazole. Oxadiazole compounds and hydrazine compounds both have shown high antifungal activity against all fungal strain except *Aspergillus fumigatus*.

3.12. Antibacterial activity

Antibacterial activity of all synthesized compounds (1 mg/mL) was evaluated against bacterial species *E. coli* (Gram negative bacteria) and *B. cereus* (Gram positive bacteria) described in Table 2. The activity was determined by measuring zone of inhibition in comparison to ciprofloxacin reference agent. A good zone of inhibition was shown by all compounds against *E. coli* bacteria. OCB and TCA could not be evaluated due to not dissolving in DMSO. Data shown that THD and OHB substituted with hydroxyl group have shown potential antibacterial activity in comparison to TBA.

4. Conclusion

This work was primary aimed at converting post-consumed recyclable PET into other value-added aromatic compounds. To achieve the above aim, a series of hydrazone and oxadiazole derivatives were synthesized from TDH, which was prepared by the aminolysis of PET flakes. Further, TDH was employed as a precursor to synthesize two oxadiazole derivatives with 2-chlorobenzoic acid/4-hydroxybenzoic acid, as well as three hydrazone derivatives with 2-chlorobenzaldehyde/benzaldehyde/4-hyd roxybenzaldehyde. The structures of the compounds were characterized by UV–Vis, FTIR, NMR, and thermal analyses. Regarding the thermal analysis, all the derivatives exhibited good thermal stability. The DFT study facilitated the calculations of the thermodynamics parameters (the dipole moment, point group symmetry, and ZPVE of the compounds) in their ground states. The presence of some groups, such as –OH, in the OHB and THD, pulled electrostatic fields, which increased the dipole moments. The vibrational frequencies of the five compounds were also optimized by DFT, and corresponded to the experimental FTIR data. The OHB, TBA and THD have shown good antifungal as well as antibacterial species *in vivo*. The obtained results were coherent with *in silico analysis*. The DFT study was supported by molecular docking. The DFT study shows ZPVE and E(thermal values) for THD thereby suggesting more hydrogen bonding. Further, the molecular dockings of the compounds were studied with target proteins (GlcN-6-P and CYP15). BEs between the target protein and the synthesized ligands were calculated, and the interactions between the two were studied separately. The computational molecular docking data revealed low BEs for all the synthesized compounds, which were comparable to those of standard voriconazole, and this demonstrated their good affinities with GlcN-6-Pand CYP15. The study indicated that the compounds might be good antifungal agents. All the docked compounds exhibited low binding affinities toward GlcN-6-P. However, among them, OHB exhibited the lowest minimum BE with the formation of only one hydrogen bond with Ser604. Therefore, this study demonstrated that these compounds are potential antifungal leads.

Declaration of Competing Interest

The authors declare that they have no known competing financial interests or personal relationships that could have appeared to influence the work reported in this paper.

Acknowledgments

The authors would like to extend their sincere appreciation to the researchers supporting project number (RSP-2020/266), King Saud University, Riyadh, Saudi Arabia. Authors would like to acknowledge SAIF, Cochin, India for carrying out NMR, elemental and thermal analysis and Department of Physics, CCSU Meerut for SEM analysis.

Authors Contributions

N.T. planned, supervised, performed DFT, docking study, characterized the material and wrote the manuscript text. R.K. drafted the manuscript and figures and characterized the material. R.A. planned and supervised the experiment. S.A. performed the synthesis and experiment. S.M. planned and performed molecular docking. M.U and A.A.K. planned, characterized the material and draft the manuscript.

Appendix A. Supplementary data

Supplementary data to this article can be found online at https://doi.org/10.1016/j.jksus.2021.101739.

References

Agrawal, R., Tarannum, N., Chourasia, M., Soni, R.K., 2018. Chemical degradation of poly(ethylene terephthalate) for potential antimicrobial activity evaluation and molecular docking study. J. Polym. Environ. 26, 819–829.
Agrawal, R., Tarannum, N., Mishra, S., Soni, R.K., 2016. Synthesis, antimicrobial activity and molecular modelling of aminolysed derivative of poly (ethyleneterephthalate). Der Pharma Chem. 8, 132–139.

Akhtar, T., Hameed, S., Al-Masoudi, N.A., Loddo, R., La Colla, P., 2008. In vitro antitumor and antiviral activities of new benzothiazole and 1,3,4-oxadiazole-2-thione derivatives. Acta Pharm. 58, 135–149.
Bharadwaj, S.S., Poojary, B., Madan Kumar, S., Byrappa, K., Nagananda, G.S., Chaitanya, A.K., Zaveri, K., Yarla, N.S., Shiralgi, Y., Kudva, A.K., Dhananjaya, B. L., 2017. Design, synthesis and pharmacological studies of some new quinoline Schiff bases and 2,5-(disubstituted-[1,3,4])-oxadiazoles. New J. Chem. 41, 8568–8585.
Bakht, M.A., Yar, M.S., Abdel-Hamid, S.G., Al Qasoumi, S.I., Samad, A., 2010. Molecular properties prediction, synthesis and antimicrobial activity of some newer oxadiazole derivatives. Eur. J. Med. Chem. 45, 5862–5869.
Bansal, S., Bala, M., Suthar, S.K., Choudhary, S., Bhattacharya, S., Bhardwaj, V., Singla, S., Joseph, A., 2014. Design and synthesis of novel 2-phenyl-5-(1,3-diphenyl-1H-pyrazol-4-yl)-1,3,4-oxadiazoles as selective COX-2 inhibitors with potent anti-inflammatory activity. Eur. J. Med. Chem. 80, 167–174.
Bondock, S., Adel, S., Etman, H.A., Badria, F.A., 2012. Synthesis and antitumor evaluation of some new 1,3,4-oxadiazole-based heterocycles. Eur. J. Med. Chem. 48, 192–199.
Becke, A.D., 1993. Density-functional thermochemistry. III. The role of exact exchange. Int. J. Chem. Phys. 98, 5648–5652.
Chmara, H., Andruszkiewicz, R., Borowski, E., 1984. Inactivation of glucosamine-6-phosphate synthetase from Salmonella typhimurium LT 2 SL 1027 by N beta-fumarylcarboxyamido-L-2,3-diamino-propionic acid. Biochem. Bioph Res Commun. 120, 865–872.
El Mejjatti, A., Harit, T., Riahi, A., Khiari, R., Bouabdallah, I., Malek, F., 2014. Chemical recycling of poly(ethylene terephthalate). Application to the synthesis of multiblock copolyesters. eXPRESS Polym. Lett. 8, 544–553.
Fukushima, K., Lecuyer, J.M., Wei, D.S., Horn, H.W., Jones, G.O., Al-Megren, H.A., Alabdulrahman, A.M., Alsewailem, F.D., McNeil, M.A., Rice, J.E., Hedrick, J.L., 2013. Advanced chemical recycling of poly(ethylene terephthalate) through organocatalytic aminolysis. Polym. Chem. 4, 1610–1616.
Fahim, A.M., Yakout, E.S.M.A., Farag, A.M., Nawwar, G.A.M., 2016. Synthesis, biological evaluation of 1,3,4-oxadiazole, triazole and uracil derivatives from poly (ethylene terephthalate) waste. Egypt. J. Chem. 59, 285–303.
Farghaly, A.A., Bekhit, A.A., Young Park, J.i., 2000. Design and synthesis of some oxadiazolyl, thiadiazolyl, thiazolidinyl, andthiazolyl derivatives of 1H-pyrazole as anti-inflammatory antimicrobial agents. Arch Pharm Med. Chem. 333, 53–57.
Frisch, M. et al. 2004.Gaussian 03, revision D. 01. Gaussian Inc.: Wallingford, CT 26.
Gaabour, L.H., 2017. Spectroscopic and thermal analysis of polyacrylamide/chitosan (PAM/CS) blend loaded by gold nanoparticles. Results Phys. 7, 2153–2158.
Karpati, L., Fejer, M., Kalocsai, D., Molnar, J., Vargha, V., 2019. Synthesis and characterization of isophorondiamine based epoxy hardeners from aminolysis of PET. Synthesis and characterization of isophorondiamine-based epoxy hardeners from aminolysis of PET. eXpress Polym. 13, 618–631.
Kazi, S.A., 2014. Synthesis and characterization of 5-substituted- (2-methylbenzimidazol-1-yl)-1,3,4-oxadiazole-2-thione and its metal complexes of Fe(III), Hg(II), Zn(II) and Sn(II). Chem. Sci. Trans. 3, 796–804.
Kaymakçıoğlu, B.K., Rollas, S., 2002. Synthesis, characterization and evaluation of antituberculosis activity of some hydrazones. II Framaco 57, 595–599.
Kohn, W., Sham, L.J., 1965. Self-consistent equations including exchange and correlation effects. Phys. Rev. 140, A1133–A1138.
Milewski, S., Chmara, H., Andruszkiewicz, R., Borowski, E., Zaremba, M., Borowski, J., 1988. Antifungal peptides with novel specific inhibitors of glucosamine 6-phosphate synthase. Drugs Exp. Clin. Res. 14, 461–475.
Mishra, K., 2014. Synthesis and antimicrobial evaluation of novelisatin derivatives. Inter. Arch. App. Sci. Technol. 5, 28–33.
Palekar, V.S., Damle, A.J., Shukla, S.R., 2009. Synthesis and antibacterial activity of some novel bis-1,2,4-triazolo[3,4-b]-1,3,4-thiadiazoles and bis-4-thiazolidinone derivatives from terephthalic dihydrazide. Eur. J. Med. Chem. 44, 5112–5116.
Parab, Y.S., Shukla, S.R., 2013. Microwave synthesis and antibacterial activity of 1,4-Bis (5-aryl-1,3,4-oxadiazole-2-yl) benzene derivatives from terephthalic dihydrazide obtained through aminolysis of PET bottle waste. Waste Biomass Valor. 4, 23–27.
Patel, S.S., Chandna, N., Kumar, S., Jain, N., 2016. I_2 mediated synthesis of 5-substituted-3-methyl/benzyl-1,3,4-oxadiazol-2(3H)-ones via sequential condensation/oxidative cyclization and rearrangement. Org. Biomol. Chem. 14, 5683–5689.
Popiołek, Ł., 2017. Hydrazide–hydrazones as potential antimicrobial agents: overview of the literature since 2010. Med. Chem. Res. 26, 287–301.
Ragaert, K., Delva, L., Van Geem, K., 2017. Mechanical and chemical recycling of solid plastic waste. Waste Manage. 69, 24–58.
Rollas, S., Küçükgüzel, S., 2007. Biological activities of hydrazone derivatives. Molecules 12, 1910–1939.
Rollas, S., Gulerman, N., Erdeniz, H., 2002. Synthesis and antimicrobial activity of some new hydrazones of 4-fluorobenzoic acid hydrazide and 3-acetyl-2,5-disubstituted-1,3,4-oxadiazolines. IL Framaco 57, 171–174.
Sulyman, M., Haponiuk, J., Formela, K., 2016. Utilization of recycled polyethylene terephthalate (PET) in engineering materials: a review. Int. J. Environ. Sci. Dev. 7, 100–108.
Sinha, V., Patel, M.R., Patel, J.V., 2010. Pet waste management by chemical recycling: a review. J. Polym. Environ. 18, 8–25.
Shukla, S.R., Harad, A.M., 2006. Aminolysis of polyethylene terephthalate waste. Polym. Degrad. Stab. 91, 1850–1854.
Saeed, A., Arshad, I., Flörke, U., 2013. Synthesis, crystal structure, and DFT study of N′-(2,4-dinitrophenyl)-2-fluorobenzohydrazide. J. Chem., 1–5
Sarojini, B.K., Krishna, B.G., Darshanraj, C.G., Bharath, B.R., Manjunatha, H., 2010. Synthesis, characterization, in vitro and molecular docking studies of new 2,5-dichloro thienyl substituted thiazole derivatives for antimicrobial properties. Eur. J. Med. Chem. 45, 3490–3496.
Teotia, M., Tarannum, N., Chauhan, M., Soni, R.K., 2019. Structure-based rational design, synthesis, crystal structure, DFT and molecular docking of 1,4 benzene dicarboxamide isomers with application as hardeners. New J. Chem. 43, 7972–7983.
Tomi, I.H.R., Al-Daraji, A.H.R., Al-Qaysi, R.R.T., Hassson, M.M., Al-Dulaimy, K.H.D., 2013. Synthesis, antimicrobial and docking study of three novel 2,4,5-triarylimidazole derivatives J. Saudi Chem. Soc.
Vanden, B.H., Koymans, L., 1998. Cytochromes P450 in fungi. Mycoses 41, 32–38.
Webb, H., Arnott, J., Crawford, R., Ivanova, E., 2013. Plastic degradation and its environmental implications with special reference to poly(ethylene terephthalate). Polymer 5, 1–18.
Wojciechowski, M., Milewski, S., Mazerski, J., Borowsk, E., 2005. Glucosamine-6-phosphate synthase, a novel target for antifungal agents. Molecular modeling studies in drug design. Acta Biochem. Pol. 52, 647–653.
Yoshida, Y., Aoyama, Y., Noshiro, M., Gotoh, O., 2000. Sterol 14-demethylase P450 (CYP51) provides a breakthrough for the discussion on the evolution of cytochrome P450 gene superfamily. Biochem. Biophys. Res. Commun. 273, 799–804.